Italian Association of Aeronautics and Astronautics
XXV International Congress
9-12 September 2019 | Rome, Italy

PRELIMINARY TAKE-OFF ANALYSIS AND SIMULATION FOR A PRANDTLPLANE COMMERCIAL AIRCRAFT

Abu Salem K.*, Palaia G.*, Bianchi M., Zanetti D.**, Cipolla V.*, Binante V.**

*University of Pisa, Department of Civil and Industrial Engineering, Pisa (Italy)

**SkyBox Engineering S.r.l., Pisa (Italy)

Abstract

The paper describes the take-off performances and characteristics of an unconventional aircraft, called PrandtlPlane. The PrandtlPlane has a box-wing architecture, founded on the "Best Wing System" concept due to L. Prandtl, that minimizes the induced drag once wingspan and lift are given. This configuration has the potential to be a more efficient alternative to conventional tube-and-wing aircraft, and it is under investigation in the framework of the PARSIFAL project, funded by the European Union in the Horizon 2020 program. A numerical simulation tool for the take-off dynamics of the aircraft, based on the non-linear equations of motion, has been developed in order to evaluate the performance of the aircraft in take-off condition. The VLM solver has been integrated into this tool in order to evaluate the aerodynamic performance of the aircraft in ground effect at each moment of the manoeuvre. The same assessments have been made for a conventional tube-and-wing reference aircraft, with the aim of conducting a performance comparison with the reference PrandtlPlane. The preliminary results obtained show the aerodynamic and aeromechanical advantages of the reference PrandtlPlane, in terms of runway length and passenger comfort.

List of Symbols

C_L	Lift coefficient	
C_{Lmax}	Max lift coefficient	
$C_{L\alpha}$	Derivative of lift coefficient respect to angle of attack	1/rad
$C_{L\delta e}$	Derivative of lift coefficient respect to elevator deflection	1/rad
$C_{L\delta f}$	Derivative of lift coefficient respect to flap deflection	1/rad
C_m	Pitching-moment coefficient	
C_{m0}	Pitching-moment coefficient at zero angle of attack	
$C_{m\alpha}$	Derivative of pitching moment coefficient respect to angle of attack	1/rad
$C_{m\delta e}$	Derivative of pitching moment coefficient respect to elevator deflection	1/rad
$C_{m\delta f}$	Derivative of pitching moment coefficient respect to flap deflection	1/rad
α	Angle of attack	rad
δ_e	Deflection angle of elevators	rad
δ_f	Deflection angle of flap	rad
V_R	Rotation speed	m/s
W	Aircraft weight	N
g	Acceleration of gravity	m/s^2
V	Speed	m/s
T	Thrust	N
D	Drag	N
R_T	Vertical reaction of the ground	N

$\mathbf{R_N}$	Horizontal reaction of the ground	N
L	Lift	N
μ	Friction coefficient	
θ	Attitude angle	rad
d	Center of gravity-wheels horizontal distance	m
h	Center of gravity-wheels vertical distance	m
$\mathbf{I_Y}$	Moment of inertia	kgm^2
$\mathbf{M_A}$	Aerodynamic moment	Nm
$\mathbf{V_Z}$	Vertical speed	m/s
γ	Trajectory angle	rad
$\mathbf{V_2}$	Take-off end speed	m/s
$\mathbf{V_1}$	Decisional speed	m/s
BFL	Balanced field length	m
$\mathbf{(X_I\ Y_I\ Z_I)}$	Initial coordinates of main surfaces	m
$\mathbf{(X_F\ Y_F\ Z_F)}$	Final coordinates of main surfaces	m
$\mathbf{\delta_Z}$	Height	m
FG	Flap Gain	
FAR	Federal Aviation Regulations	
$\mathbf{n_Z}$	Vertical load factor	
MTOW	Maximum Take-Off Weight	N

Introduction

The aviation demand growth is around 4.5% per year [1][2], and it is foreseen to double in a couple of decades [3]; this trend will be accompanied by the saturation of most of the airports worldwide and an unacceptable increment of air pollution in the atmosphere with a consequent greenhouse effect [4][5]. The requirements by ACARE [6] of cutting the CO_2 and NO_X pollutions and reducing significantly the external noise around the airport areas will be hardly satisfied by improving the conventional tube-and-wing aircraft, so the introduction into service of disruptive aerodynamic configurations is seriously considered a possible solution for obtaining a greener and more efficient air traffic in the future. Different innovative aerodynamic configurations [7] have been proposed for the civil aviation of the future as, in particular, Blended Wing Body, Truss Braced Wings, and PrandtlPlane [8]. To investigate these unconventional configurations, in Europe, in the framework of Horizon 2020, a call named "breakthrough innovation in aeronautics" has been devoted to finance cooperative projects to design a "disruptive aircraft" for future air traffic. The project "PARSIFAL" (Prandtlplane ARchitecture for the Sustainable Improvement of Future AirpLanes), funded by the European Community, aims at designing an innovative aircraft, based on the adoption of the PrandtlPlane configuration (in honour of L. Prandtl), and also to compare the performances with those of conventional reference aircraft. The lifting system of the PrandtlPlane configuration is a box-wing in the front view, according to the Prandtl's Best Wing System concept [10]. As is well known, this configuration minimizes the induced drag among all the possible lifting systems with the same total lift and the same span [9]. PARSIFAL project aims at demonstrating that the application of the PrandtlPlane configuration to aircraft with the same overall dimensions of short-medium range aircraft, in particular with wingspan below 36 m, can increase the payload capacity from less than 200 up to more than 300 passengers, hence with a significant reduction of environmental impact and direct costs per passenger. Understanding the performance is mandatory for this new architecture, especially for the take-off phase. It is well known in literature [11][12] that during the take-off phase the aircraft is subject to a phenomena called "ground effect" which helps the aircraft, but it can be unfavourable in the landing phase. The ground effect, in the case of a

PrandtlPlane, could influence the aerodynamic characteristics in take-off more than for conventional aircraft, because there are two wings positioned at different heights, and the front one is very close to the runway. The main goal of this paper is to address how the take-off performance of the PrandtlPlane are affected by the main design parameters in order to define the main performances in terms of balanced field length and decisional speed. More in details, in the first part of the paper two-reference aircraft are described: one is a PrandtlPlane aircraft and one is a conventional tube-and-wing configuration. A common procedure for movables sizing is then described, together with the aerodynamic evaluation methods adopted in this work. Then, the dynamic simulation modelling and the mathematical model are defined; in the final part, the main results of the simulation are shown, focusing on the comparison between the take-off performance of the two reference aircraft. Since the lack of information available in literature regarding the analysis of the PrandtlPlane in take-off condition, another objective of the present activity is to provide design tools to be used in the final optimisation of the aircraft.

1. Reference aircraft

Two different configurations have been considered in this work: one is a conventional tube-and-wing configuration, and the second one is a PrandtlPlane. The reference PrandtlPlane aircraft is called MS1 and represents the result of the first period of the design activities in PARSIFAL project; detailed description of this configuration is in [13],[14],[15],[17]. The drawings of this configuration and its main characteristic are reported in Figure 1.

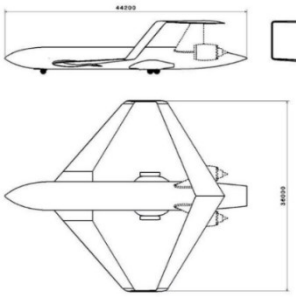

Parameter	Symbol	Value	Unit
Maximum take-off weight	W	$1,218 \cdot 10^5$	kg
Moment of inertia	I_y	$1,298 \cdot 10^7$	kg m^2
Wing surface	S_{ref}	266,7	m^2
Span	b	36	m
Mean aerodynamic chord	$\bar{c}$	4,32	m
Maximum thrust-to-weight ratio	T_{max}/W	0,3	–

Figure 1 Three views of the MS1 PrP configuration

One of the main objectives of the present analysis is understanding how the take-off performance of the reference Prandtlplane configuration differs from that of a conventional aircraft. The main competitors of the PARSIFAL PrP aircraft are represented by the short-medium range conventional aircraft [17], as the Airbus A320 or the Boeing 737. In this work the reference conventional aircraft chosen for the performance comparison is the CeRAS CSR01 [18], a public reference model for short-medium aircraft. The CeRAS CSR01 drawings and its main characteristic are reported in Figure 2.

In order to evaluate and to compare the take-off performance of these two configurations, it has been necessary to define a common sizing procedure of high-lift devices and control surfaces. Indeed, the low speed performances, such as those in take-off (i.e. stall speed and C_{Lmax}), are strictly related to the design of these components. A preliminary sizing procedure for both elevators and

flaps has been defined and it is described in [13]; the procedure is based on the trim fulfilment in approach condition. The trim problem is thus defined:

$$\begin{cases} C_L = C_{L\alpha}\alpha + C_{L\delta e}\delta_e + C_{L\delta f}\delta_f \\ C_{m0} + C_{m\alpha}\alpha + C_{m\delta e}\delta_e + C_{m\delta f}\delta_f = 0 \end{cases}$$

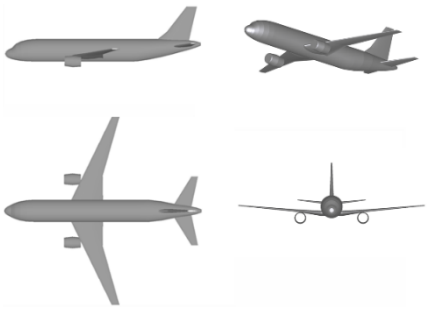

Parameter	Symbol	Value	Unit
Maximum take-off weight	W	$7,7 \cdot 10^4$	kg
Moment of inertia	I_y	$8,21 \cdot 10^6$	kg m^2
Wing surface	S_{ref}	$122,4$	m^2
Span	b	34.07	m
Mean aerodynamic chord	$\bar{c}$	$4,18$	m
Maximum thrust-to-weight ratio	T_{max}/W	$0,3$	–

Figure 2 Three views of the CeRAS configuration

For the PrandtlPlane there are many possible layout for positioning the movables; the one selected for the current analyses is represented in Figure 3 (right): the elevators are placed in the root regions of both wings, the ailerons are installed in the tip regions and the flaps are placed between the elevators and the ailerons. Front and rear elevators are actuated with opposite deflections in order to introduce ideally a pitching moment without affecting the total lift. For the tube-and-wing aircraft, the layout is the conventional one, with the elevators placed on the horizontal tailplane and the flap

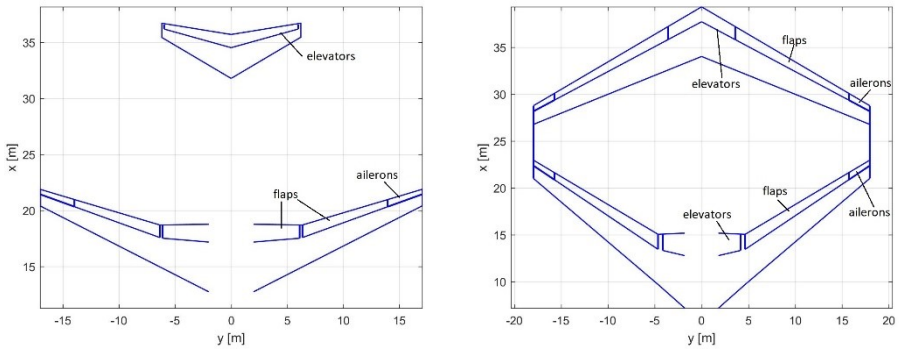

Figure 3 Movables layout for the two configurations

on the main wing, as sketched in Figure 3 (left).The trim problem is solved by using the AVL code; the flap deflection is set as an input, and the aerodynamic solver finds α and δ_e in order to fulfil vertical and pitch equilibrium in approach condition, at Maximum Landing Weight. Due to the limitations of the AVL solver, all the movables are considered as plain flap (also the high-lift devices). At the end, the low speed performance of the configurations designed with these procedures are estimated by means of consolidated literature methods, as [19]. The whole procedure is schematized in Figure 4.

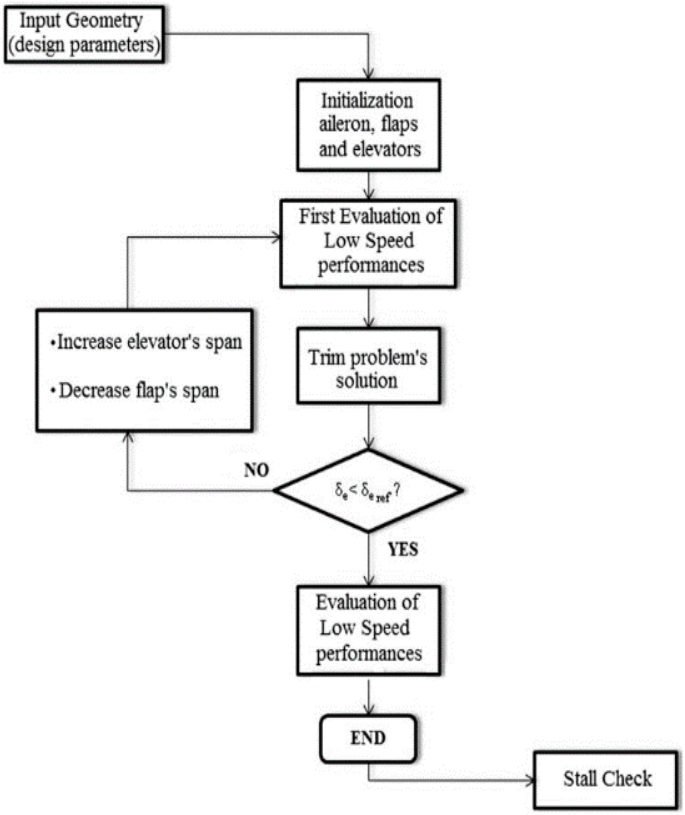

Figure 4 Preliminary sizing procedure for control surfaces and high-lift devices

2. Simulation modelling

It is possible to divide the take-off manoeuvre in three different segments: ground-roll, rotation, and transition to climb, as sketched in Figure 5. In the ground roll segment, the aircraft starts its take-off acceleration and reaches the rotation speed (V_R); the only degree of freedom is the longitudinal motion of the aircraft on the runway. The rotation segment starts when the V_R speed is reached and consists in the rotation of the aircraft around the main landing gear; this stage terminates when the aircraft pulls the wheels off the ground. Then, in the transition to climb phase, the aircraft follows a near circular path followed by the subsequent climb segment. According to Federal Aviation Regulations (FAR), at the end of the runway the aircraft must reach a minimum height of 35 ft, (called "screen height") and, at that point, its speed cannot be lower than 1.2 times the stall speed with flaps extracted.

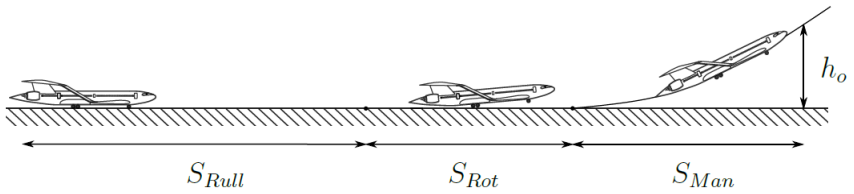

Figure 5 Take-off manoeuvre

2.1 Equations of motion

Following the forces schemes for the three take-off phases reported in Figure 6, the equations of motion can be written as follows:

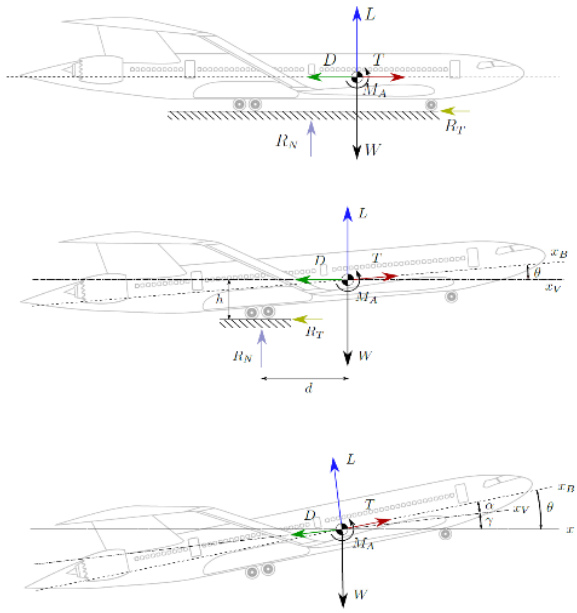

Figure 6 Forces schema for the three take-off segments

Ground Roll:

$$\begin{cases} \frac{W}{g}\frac{dV}{dt} = T - D - R_T \\ R_N + L = W \\ R_T = \mu R_N \end{cases}$$

Rotation:

$$\begin{cases} \frac{W}{g}\frac{dV}{dt} = T\cos\theta - D - R_T \\ I_y\frac{d^2\theta}{dt^2} = M_A - R_N d - R_T h \\ R_N + L = W \\ R_T = \mu R_N \end{cases}$$

Lift off:

$$\begin{cases} \frac{W}{g}\frac{dV}{dt} = T\cos\theta - D\cos\gamma - L\sin\gamma \\ \frac{W}{g}\frac{dV_z}{dt} = T\sin\theta - D\sin\gamma - L\cos\gamma \\ I_y\frac{d^2\theta}{dt^2} = M_A \end{cases}$$

The ordinary differential equations of motion are non-linear, and the degrees of freedom are strongly coupled so that no closed-form solution is possible; thus, it has been necessary to provide numerical solutions. The integration is conducted with the Euler Method with a time step of 10^{-2} seconds; due to the implementations of the aerodynamic evaluations in each step of the integration, the method has a high computational cost.

2.2 Mathematical model for the aircraft geometry evaluation with respect to attitude variation

As described in section 2.1, the take-off manoeuvre is composed of three parts: ground-roll, rotation, and lift-off. During the first phase the aircraft attitude does not change, whereas in the second and third phases attitude and height change. The main differences between the two last phases is the position of the instant centre of rotation: during the rotation phase, it is the contact point between the tires of the main landing gear and the ground; in the lift-off phase, it is the centre of gravity. The aircraft-ground relative position has to be evaluated accurately in order to estimate the aerodynamic coefficients in ground effect, so a proper mathematical model has been developed.

Rotation

Exceeding the V_R speed, the aircraft deflects the elevator and pitches-up around the ground-tire contact point. The rotation comes around an axis parallel to the pitch axis, so there is a symmetry respect to its longitudinal plane, and an easy formulation can be obtained without losing generality. The reference system has the origin in the nose of the aircraft and, after the rotation, all coordinates of the main surfaces (e.g. wings and fuselage) change. Indicating with X_F, Y_F, and Z_F the new coordinates in the reference system (τ) and with X_I, Y_I, and Z_I the initial coordinates in τ, we obtain:

$$\begin{bmatrix} X_F \\ Y_F \\ Z_F \end{bmatrix} = \begin{bmatrix} \cos\theta & 0 & \sin\theta \\ 0 & 1 & 0 \\ -\sin\theta & 1 & \cos\theta \end{bmatrix} \begin{bmatrix} X_I - X_R \\ Y_I \\ Z_I - Z_R \end{bmatrix} + \begin{bmatrix} X_R \\ 0 \\ Z_R \end{bmatrix}$$

The coordinates X_R and Y_R indicate the position of the instant centre of rotation; θ indicates the rotation of the aircraft.

Lift-off

When the aircraft lift off from ground, the centre of gravity becomes the new instant centre of rotation. The equations are similar to the previous ones, but we have to take into account the relative distance ground-centre of gravity (δ_Z).

$$\begin{bmatrix} X_F \\ Y_F \\ Z_F \end{bmatrix} = \begin{bmatrix} \cos\theta & 0 & \sin\theta \\ 0 & 1 & 0 \\ -\sin\theta & 1 & \cos\theta \end{bmatrix} \begin{bmatrix} X_I - X_R \\ Y_I \\ Z_I - Z_R \end{bmatrix} + \begin{bmatrix} X_R \\ 0 \\ Z_R + \delta_Z \end{bmatrix}$$

All these coordinates allow to define the new geometry in order to evaluate the aerodynamic coefficient in ground effect with AVL.

2.3 Evaluation of aerodynamic coefficients

The aerodynamic characteristics of an aircraft during take-off are strongly influenced by the ground effect, whose main consequences are a significant reduction of the induced drag (due to the modifications of tip vortices and downwash), and an increase of the lift-generating capabilities, also

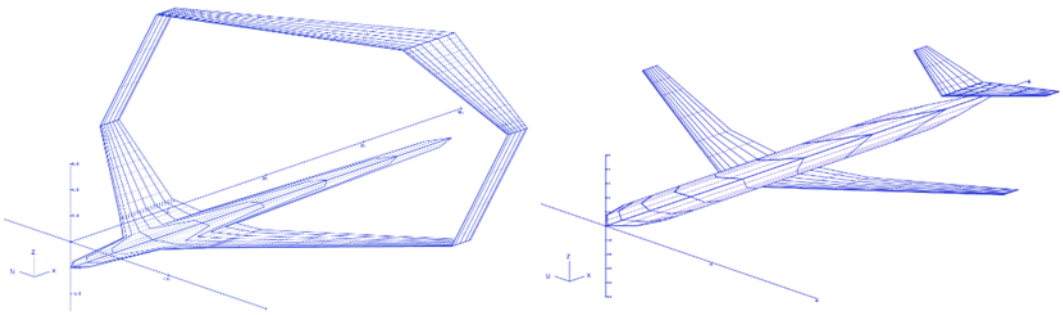

Figure 7 MS1 (left) and CeRAS (right) AVL models

referred as “air cushion” [11][12]. The ground effect depends on the aerodynamic characteristics of the aircraft and, in particular, on the clearance of the wings from the ground. For this reason, in order to realistically simulate the aerodynamics of the aircraft during the take-off phase, it has been decided to evaluate the aerodynamic characteristics in each time step considered; in fact, the position of the aircraft with respect to the ground varies during the evolution of the manoeuvre, depending on the variables z(t) and θ(t), as described in paragraph 2.2. Given the large number of aerodynamic evaluations to be done for each simulation, the computation of the aerodynamic characteristics has been carried out using low-fidelity codes, with the aim of limiting the computational time. In particular, the potential AVL code, based on the Vortex Lattice Method, has been used; with the AVL code, the evaluation of ground effect has been studied by specifying the symmetry of the aircraft with respect to the ground plane. A validation procedure to assess the accuracy of AVL when simulating ground effect has been presented in [20]. The AVL models for the MS1 and CeRAS configuration are shown in Figure 7. The main differences between the two configurations that affect the aerodynamics in ground effect consist, obviously, in the shape of the lifting systems (boxwing vs monoplane), and the engine installation, that influences the ground clearance of the aircraft. In the case of the MS1 PrandtlPlane configuration, the front wing is very

close to the runway, because of the fuselage-mounted engine; in the case of a conventional tube and wing aircraft, the main wing has a larger distance from the runway, due to the wing-mounted engine.

In the following figures the main aerodynamic coefficients (evaluated with AVL considering ground effect) are reported for the MS1 and CeRAS configurations with respect to α and height (z) variations. The graphs in Figure 9 show the increase in the lift coefficient as the aircraft approaches the ground, for both configurations. This is mainly due to the presence of ventral overpressures on

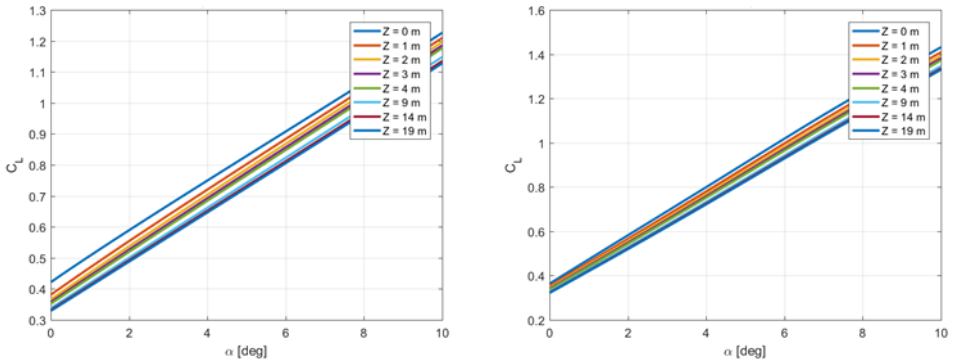

Figure 9 C_L curves for MS1(left) and CeRAS (right) at clean configuration (δ_e=δ_f=FG=0)

the lifting surfaces that causes an increase in the lift generated (effect known as 'air cushion'). Smaller the distance between the lifting surface considered and the ground, larger the effect. For this reason, the MS1 configuration has a better advantage from the point of view of lift in ground effect, due to the fact that the front wing (that is the more loaded between the two wings of the boxwing) is much closer to the ground than the monoplane competitor. Moving from an altitude of 20 meters (calculated with respect to the centre of gravity of the aircraft) to an altitude of 0 meters, and with a zero attitude angle, there is a gain in lift coefficient of 28% for the PrandtlPlane, while for the conventional aircraft, under the same conditions, there is an increase of 13%. The better performance in ground effect for the boxwing is also evident in terms of $C_{L\alpha}$, as shown in *Figure 8*. Compared to the free air flight condition, the PrP configuration has a gain in $C_{L\alpha}$ equal to 33%

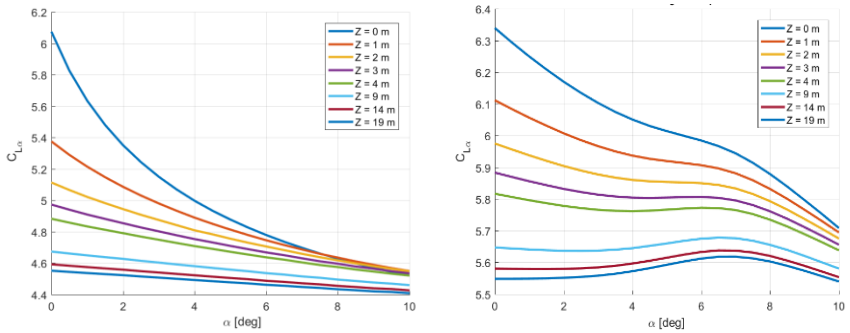

Figure 8 $C_{L\alpha}$ curves for MS1(left) and CeRAS (right) at clean configuration (δ_e=δ_f=FG=0)

during ground roll, while for the competitor tube-and-wing is only of 14%.

The $C_{L\alpha}$ is not constant with α for configurations that are affected by the ground effect; the graph in Figure 8 shows that lifting performance decreases with the increase in aircraft angle of attack: it is due to the distance increase between the wing (in particular the front wing for boxwing) and the runway.

The second significant effect of the proximity of the aircraft to the runway is the reduction of induced drag, as can be seen from the C_{Di} graphs, shown in Figure 10. Also for this aspect, the ground effect performance of the PrandtlPlane is better than the CeRAS; moving from free air to ground roll, the C_L/C_{Di} ratio increases by 87% for the PrP and 38% for the monoplane.

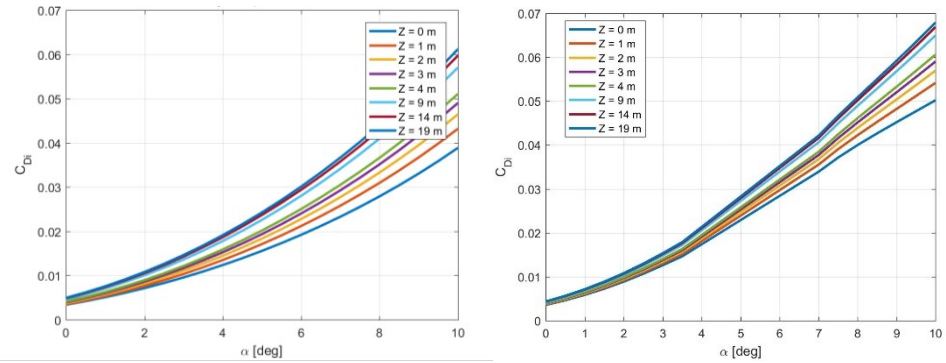

Figure 10 CDi-α curves for MS1(left) and CeRAS (right) at clean configuration (δ_e=δ_f=FG=0)

For the PrP MS1 configuration, as the incidence increases (and therefore in the rotation phase in the case of a take-off manoeuvre), the front wing moves away from the ground while the rear wing approaches, causing a pitch stiffening, as can be read from the $C_{m\alpha}$-α graph in Figure 11; increasing the distance of the aircraft from the runway, this effect tends to disappear. For the monoplane, the greater proximity to the ground causes an increase in pitch stiffness due to the increase in the lift capacity of the main wing.

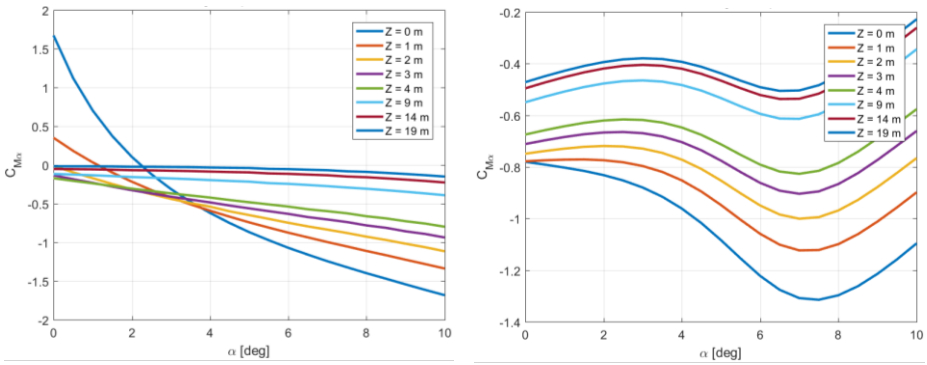

Figure 11 $C_{m\alpha}$-α curves for MS1(left) and CeRAS (right) at clean configuration (δ_e=δ_f=FG=0)

3. Simulation results

3.1 Definition of BFL according to FAR

The evaluation of the balanced field length (BFL) is crucial for the aircraft performance in the take-off phase. According to FAR, two "main distances" are fundamental for the evaluation of the decisional speed (balanced V_1) and the BFL: the Take-Off Distance (TOD) and the Accelerate-Stop Distance (ASD). In this work only dry runway is considered.

According to FAR 25.113 the TOD on a dry runway is the greater of:

a) The horizontal distance (TOD_{N-1}) along the take-off path from the start of take-off to the point at which the airplane is 35 feet above the take-off surface. During the take-off path an

engine failure occurs and is recognized at V_1 (delayed of one second respect to engine failure speed [21])

b) The 115 percent of the horizontal distance (TOD_N) along the take-off path, with all engine operating, from the start of take-off to the point at which the airplane is 35 feet above the take-off surface.

The first condition is related to a take-off with one engine inoperative (OEI); the second one is related to a take-off with all engine operative (AEO). The above requirement can be expressed as

$$TOD = \max \{TOD_{N-1}, TOD_N\}$$

Bigger the V_{EF} (engine failure speed), shorter the runway; this is due to the fact that an increase of V_1 (i.e. V_{EF}) allows to reduce the distance covered in the ground-roll phase.

According to FAR 25.109 the ASD on a dry runway is the greatest of:

The sum of the distances (ASD_{N-1}) necessary to

a) Accelerate the airplane from a standing start with all engines operating to V_{EF};
b) Allow the airplane to accelerate from V_{EF} until V_1 with one engine operating;
c) Come to a full stop plus a distance equivalent to two seconds at V_1.

The sum of the distances (ASD_N) necessary to

a) Accelerate the airplane from a standing start with all engines operating to V_1;
b) Come to a full stop plus a distance equivalent to two seconds at V_1.

The above regulation can be expressed as

$$ASD = \max \{ASD_{N-1}, ASD_N\}$$

Higher the V_1, longer the runway; this is due to that an increase of V_1 raises the distance covered in the acceleration phase, the deceleration phase, and the distance covered at V_1 for two seconds.

3.2 Design parameters: δ_{flap}, W_{TO}, (FG),

The main parameters for the take-off analysis of the PrandtlPlane are: flap deflection, take-off weight, and the Flap Gain, which is defined as the ratio between the rear wing flap deflection ($\delta_{flap-post}$) and front wing flap deflection ($\delta_{flap-ant}$). Therefore, chosen the front flap deflection among the values [10° 20° 30°], the rear flap deflection is given by

$$\delta_{flap-post} = FG \times \delta_{flap-ant}$$

The rotation speed follows FAR 25.107, according to which V_R has to be higher than V_1 and has to guarantee the reaching of V_2. For the CeRAS take-off analysis, all the above parameters are set equal, except for the flap gain, which cannot be defined for a conventional tube-and-wing configuration.

3.2 BFL - Main results

In this section the results of the take-off simulations, in terms of BFL and V_1, are presented. First of all, the performance of the MS1 PrandtlPlane configuration are discussed; the first parameter analysed is the Flap Gain. In Figure 12 the curves of the completed take-off manoeuvre (solid lines) and of the aborted take-off manoeuvre (dashed lines) in case of an engine failure at the corresponding speed $V_{failure}$ are reported. The take-off distances X_{TO} are given in meters and the speeds in m/s. From these results, also reported in the following Table 1 for front wing δ_{flap_ant}=20°

and δ_{flap}=30°, it clearly follows that increasing the rotation of the rear flap is penalizing in terms of balanced take-off distance, while using the rear plain flap in counter-rotation gives a small gain with respect to the case of clean rear wing.

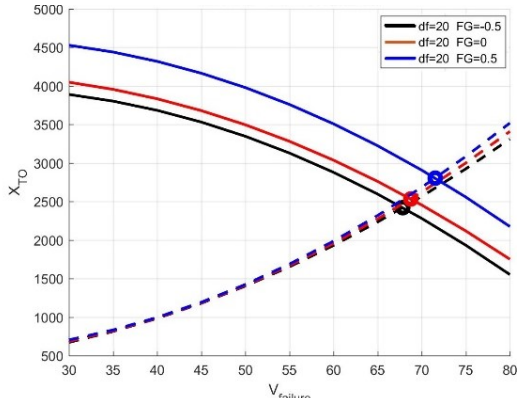

Figure 12 BFL and V_1 for the MS1 varying FG at δ_{flap}=20°

%W_{TO}	$\delta_{flap\ ant}$ [deg]	FG	V_1 [m/s]	BFL [m]
100	20	-0.5	67	2420
100	20	0	68	2530
100	20	0.5	71	2810

%W_{TO}	$\delta_{flap\ ant}$ [deg]	FG	V_1 [m/s]	BFL [m]
100	30	-0.5	64	2180
100	30	0	65	2290
100	30	0.5	68	2640

Table 1 BFL and balanced V_1 for the MS1 varying FG

The reason of these trends relies on the specific architecture and balance of the MS1 configuration: giving a positive flap rotation to the rear plain flap increases the pitch down moment that is in contrast to the elevator action necessary for the aircraft rotation (Figure 13, left). The graphs depicted in Figure 13 show some relevant take-off parameters of a generic MS1 take-off manoeuvre (without failures). Moreover, a positive rear flap rotation increases the total drag force during the ground roll acceleration (Figure 13, centre). However, in the following discussion of the results, the reference value of FG is set equal to zero; negative FG, in fact, may lead to high values of attitude angles θ (Figure 13, right) that may be incompatible with the tail-clearance requirements for the

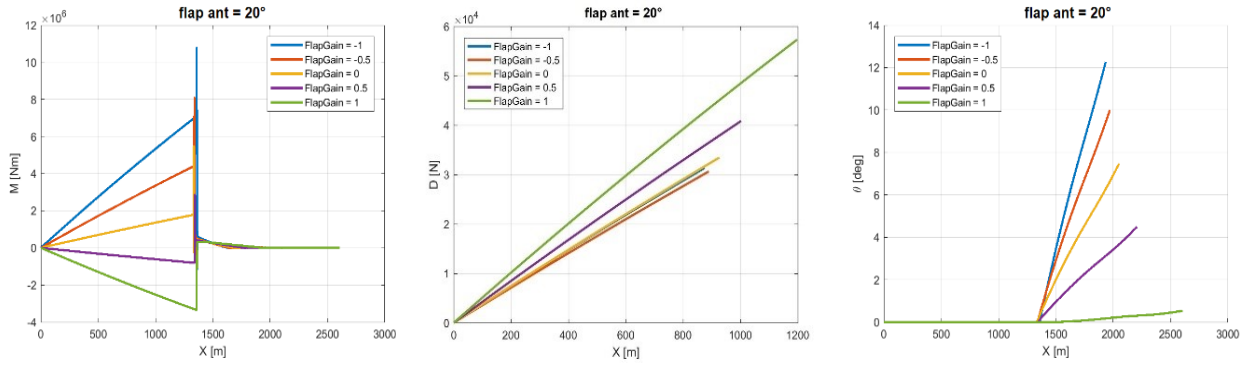

Figure 13 Pitching moment (left), ground roll drag (center), attitude (right) for a generic take-off maneuver for the MS1 varying FG

aircraft during the rotation phase.

The second main parameter that influences the take-off performance is the δ_{flap}; this parameter, consequently to the definition of the FG parameter, has to be intended referred to the front wing flap. In the graphs of Figure 14 are represented the balanced take-off length for the MS1 configuration, varying the δ_{flap} parameter; the same results are reported in, for two different values of FG. It can be noted that, for both the FG considered, the runway length requested for the take-off decreases when the δ_{flap} increases.

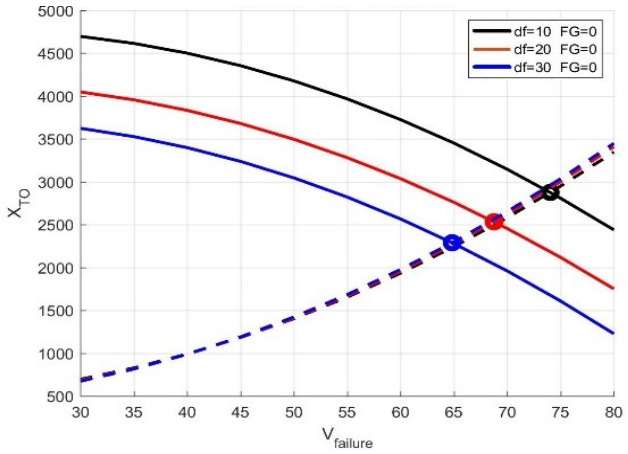

Figure 14 BFL and V_1 for the MS1 varying δ_{flap} for FG = 0

$\%W_{TO}$	$\delta_{flap\ ant}$ [deg]	FG	V_1 [m/s]	BFL [m]
100	10	0	74	2870
100	20	0	68	2530
100	30	0	64	2290

$\%W_{TO}$	$\delta_{flap\ ant}$ [deg]	FG	V_1 [m/s]	BFL [m]
100	10	0.5	75	3050
100	20	0.5	71	2810
100	30	0.5	68	2640

Table 2 BFL and balanced V_1 for the MS1 varying δ_{flap}

An evaluation of the sensibility on the requested take-off length with respect to the take-off weight has been done; the results are reported in Figure 15 and in Table 3. The take-off weights considered are fraction of the MTOW of the MS1 configuration; as expected, the requested balanced field length is shorter for a lighter aircraft.

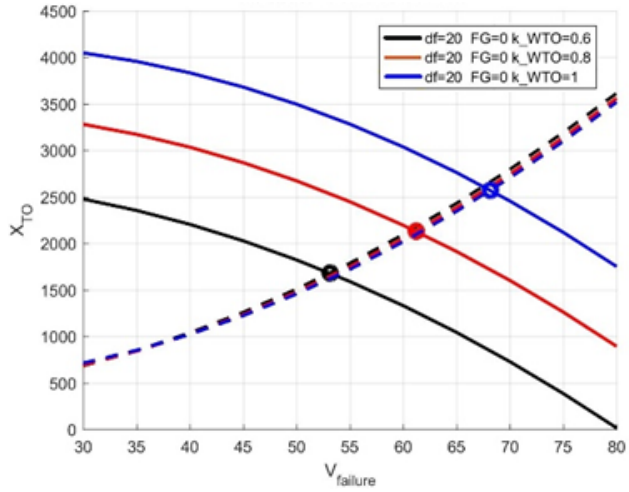

Figure 15 BFL and V_1 for the MS1 varying WTO

$\%W_{TO}$	δ_{flap} [deg]	FG	V_1 [m/s]	BFL [m]
60	20	0	53	1680
80	20	0	61	2130
100	20	0	68	2530

$\%W_{TO}$	δ_{flap} [deg]	FG	V_1 [m/s]	BFL [m]
60	30	0	51	1520
80	30	0	58	1920
100	30	0	64	2290

Table 3 BFL and balanced V_1 for the MS1 varying WTO

Following these considerations, the reference setting for the PrP MS1 configuration in take-off condition is: δ_{flap}=30°, FG=0, W_{TO}=MTOW; this reference configuration is selected in order to perform comparison with the take-off performance of the reference tube-and-wing.

For the CeRAS configuration, the evaluation of the performance in take-off condition has been done considering variations of δ_{flap} and W_{TO}. As reported in Figure 16 and Table 4, increasing the δ_{flap} value from 20° to 30° does not produce any gain in performance. This may be related to the

higher increase in drag coefficient whit respect to the increase in lift coefficient for this specific configuration with δ_{flap}=30°.

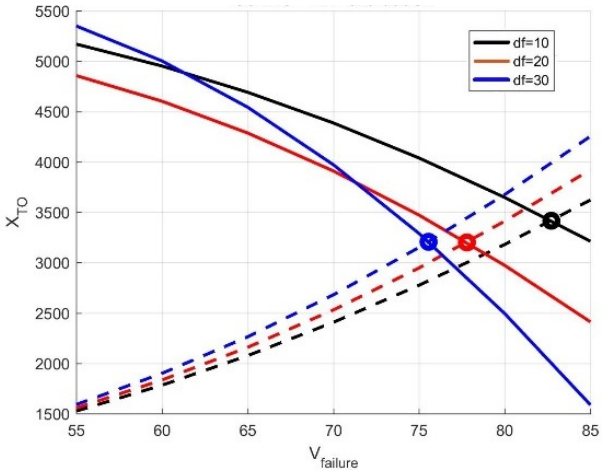

Figure 16 BFL and V_1 for the CeRAS varying δ_{flap}

$\%W_{TO}$	δ_{flap} [deg]	V_1 [m/s]	BFL [m]
100	10	82	3410
100	20	77	3200
100	30	75	3210

Table 4 BFL and balanced V_1 for the CeRAS varying δ_{flap}

As described for the MS1 configuration, also for the CeRAS reducing the take-off weight implies a reduction in balanced field length. These results are reported in Figure 17 and Table 5.

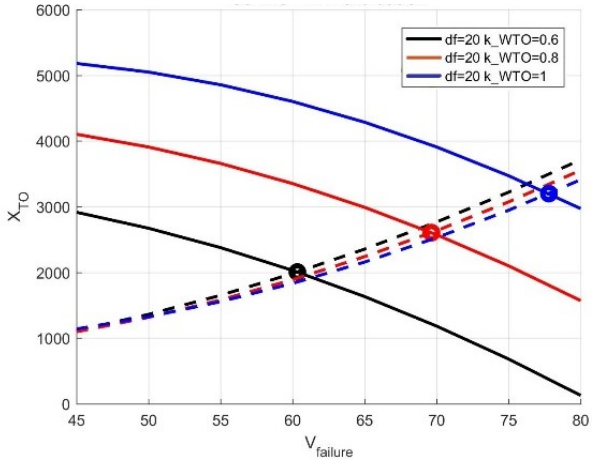

Figure 17 BFL and V_1 for the CeRAS varying WTO

$\%W_{TO}$	δ_{flap} [deg]	V_1 [m/s]	BFL [m]
60	20	60	2005
80	20	69	2610
100	20	77	3200

$\%W_{TO}$	δ_{flap} [deg]	V_1 [m/s]	BFL [m]
60	30	58	2010
80	30	67	2610
100	30	75	3210

Table 5 BFL and balanced V_1 for the CeRAS varying WTO

The reference setting for the CeRAS configuration in take-off condition is: δ_{flap}=20°, W_{TO}=MTOW. Considering the reference MS1 setting for the take-off, it is possible to notice that, for the PrP, the BFL is 28.4% shorter than the BFL requested by the CeRAS. This is mainly related to the higher aerodynamic efficiency of the Best Wing System and to the higher aerodynamic gain in ground effect of the MS1 configuration (front wing very close to the ground).

3.3 Thrust Reduction

The above results on the BFL show the shorter runway for the PrandtlPlane MS1 configuration respect to the CeRAS. Consequently, it can be reasonable to assume a thrust reduction in order to obtain comparable performances with the PrP clean configuration. The installed thrust, for PrP and CeRAS, is equal to the 30% of the MTOW, but the previous results have been obtained with a thrust-weight ratio equal to 80% of the installed thrust; in the next case, a full thrust has been considered for the CeRAS. The results plotted in Figure 18 and detailed in Table 6 show a similar performance between the two aircraft; moreover, at maximum flap deflection the BFL, for the PrP, is slightly shorter (of about 90m). Thanks to this preliminary analysis it is possible to consider, for the PrP, an engine thrust reduction of about 20%, ensuring the same performances, in terms of BFL, of the CeRAS.

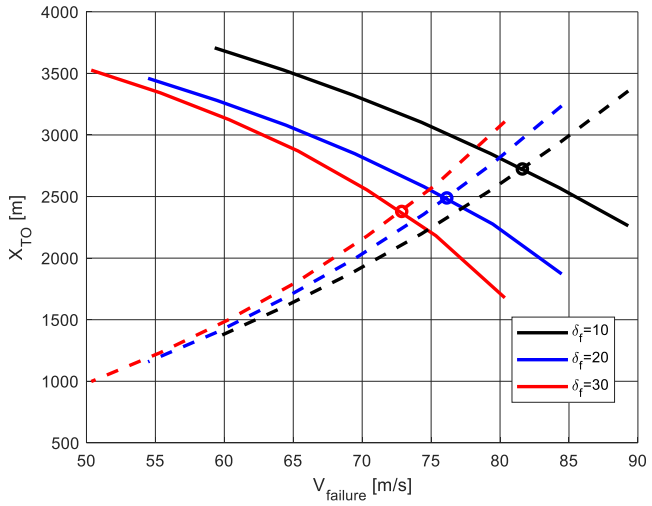

Figure 18 BFL and V1 for the CeRAS varying flap deflection at T/W=0.3

$\%W_{TO}$	δ_{flap} [deg]	V_1 [m/s]	BFL [m]
100	10	82	2724
100	20	76	2489
100	30	72	2379

Table 6 BFL and V1 for the CeRAS varying flap deflection at T/W=0.3

3.4 Standard take-off - Main results

As shown in section 3.2, a different flap deflection or flap gain setting can lead to a considerable change in BFL. Nevertheless, for a complete analysis, is necessary to focus also on standard performance, i.e. when no engine failure occurs. The conditions set for PrP and CeRAS simulations were:

1. Full thrust by the two engines for all the manoeuvre;
2. Dry runway;
3. No wind during the take-off;
4. Airport at zero altitude;
5. Standard air condition.

In this section the influence of the main parameters (δ_{flap} and FG) are presented for the PrP configuration; obviously, no flap gain was considered for the CeRAS. In order to evaluate the aircraft performance, three main quantities are considered: pitch angle at the end of the take-off and average vertical load factor (n_z) during the lift-off phase for the passenger comfort, and the length of the runway. All the data are evaluated at MTOW. The results in Table 7, Table 8, and Table 9, show for the PrP a trend for n_z: lower the flap gain higher the vertical load factor. It is reasonable to assume that this trend is due to the PrP configuration; a flap deflection of the rear wing increases the

pitching moment, and a lower incidence angle is developed, so lower lifting force and, consequently, lower n_z.

δ_{flap} [deg]	Flap gain	n_z	θ [deg]	Runway length [m]
10	-0.5	1.1	8.3	2307
10	0	1.08	6.89	2382
10	0.5	1.06	5.3	2492

Table 7 Vertical load factor, pitch angle, and runway length varying flap gain at δ_{flap} =10°

δ_{flap} [deg]	Flap gain	n_z	θ [deg]	Runway length [m]
20	-0.5	1.13	10.06	1975
20	0	1.1	7.52	2056
20	0.5	1.07	4.52	2212

Table 8 Vertical load factor, pitch angle, and runway length of PrP varying flap gain at δ_{flap} =20°

δ_{flap} [deg]	Flap gain	n_z	θ [deg]	Runway length [m]
30	-0.5	1.16	11.7	1760
30	0	1.12	8.18	1833
30	0.5	1.07	3.8	2021

Table 9 Vertical load factor, pitch angle, and runway length of PrP varying flap gain at δ_{flap} =30°

In Table 10 the results of CeRAS take-off show no influence of flap deflection on n_z and a slight influence on final pitch angle.

δ_{flap} [deg]	n_z	θ [deg]	Runway length [m]
10	1.14	7.93	2696
20	1.15	6.84	2356
30	1.15	5.84	2158

Table 10 Vertical load factor, pitch angle, and runway length of CeRAS varying δ_{flap}

Comparing PrP and CeRAS, a shorter runway length and lower n_z stand out. The differences, in percentual terms, are detailed in Table 11. For the PrP a zero Flap Gain is considered.

δ_{flap} [deg]	Δn_z [%]	Δ Runway length [%]
10	-5.2	-11.6
20	-4.3	-12.7
30	-2.6	-15.1

Table 11 Vertical load factor, pitch, and runway length comparison at FG=0

The results comparison shows a shorter runway length for the PrP; a lower vertical load factor which increases the passenger comfort, and higher pitch angle for the flap deflection of interest. Considering a flap deflection of 20° a trajectory comparison is depicted in Figure 19.

Conclusions and future developments

In this paper the preliminary take-off performance and characteristics of a PrandtlPlane aircraft have been presented. In the first part of the paper two reference configurations have been described: a reference PrandtlPlane aircraft, developed in the framework of the PARSIFAL project, and a reference tube-and-wing aircraft selected from the CeRAS database. Then the simulation of take-off dynamics has been described, followed by the description of the aerodynamic evaluation in ground effect for the two aircraft. From the preliminary analysis of the aerodynamic results it is evident that the PrandtlPlane has a higher gain on C_L, $C_{L\alpha}$, and aerodynamic efficiency (lift over drag ratio). The reason behind this behaviour is strictly related to the configuration architecture, for which the front wing is very close to the ground. The discussion of the results in terms of Balanced Field Length

analysis and standard take-off analysis is presented in the final part of the paper. From this analysis it emerges that the reference PrandtlPlane aircraft has better take-off performance with respect to the conventional competitor, both in terms of take-off runway length (mainly related to the higher aerodynamic efficiency of the reference PrandtlPlane configuration), and in terms of passenger comfort. However, the results here presented are preliminary and can be improved; in the future activities a calibration of the low-fidelity ground effect aerodynamic evaluation will be carried out, using RANS models. Then, a surrogate model will be built, in order to strongly reduce the computational time for each take-off simulation; in this way, a wider set of design parameters can be analysed, and then optimization procedures for take-off manoeuvre can be set up.

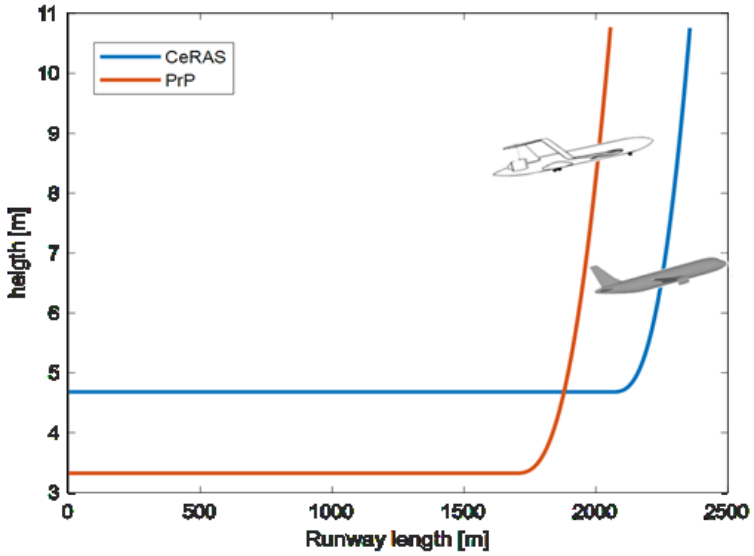

Figure 19 Centre of gravity trajectory comparison between PrP and CeRAS

Acknowledgments

The present paper concerns part of the activities carried out within the research project PARSIFAL ("Prandtlplane ARchitecture for the Sustainable Improvement of Future AirpLanes"), which has been funded by the European Union under the Horizon 2020 Research and Innovation Program (Grant Agreement n.723149).

References

[1] Airbus *Global Market Forecast 2017-2037* (Airbus Commercial Aircraft, Toulouse, 2017)
[2] Boeing *Global Market Outlook 2017-2036* (Boeing Commercial Airplanes, Seattle, 2017)
[3] PARSIFAL Project, Report on socio-economic scenarios and expectations. Deliverable 1.1, 2018, www.parsifalproject.eu
[4] Lee, D. S. et al. Aviation and global climate change in the 21st century. Atmos. Environ. 2009, Vol. 43, 3520–3537 (2009)
[5] Schäfer W.A. et al. Technological, economic and environmental prospect of all-electric aircraft. Nature energy 2019, Vol.4, 160-166
[6] ACARE. Strategic Research and Innovation Agenda (SRIA). Advisory Council for Aviation Research and Innovation in Europe, 2017, www.acare4europe.org
[7] Cavallaro R and Demasi L. Challenges, ideas, and innovations of joined-wing configurations: a concept from the past, an opportunity for the future. Prog. Aerosp Sci 2016, Vol. 87: 1–93
[8] Aldo Frediani, 2005. Swept-wing box-type aircraft with high flight static stability. European patent N. EP1597145

[9] Frediani, A. The Prandtl wing. VKI lecture series: Innovative Configurations and Advanced Concepts for Future Civil transport Aircraft, June 06-10 (2005)
[10] L. Prandtl. Induced Drag of Multiplanes",Technical Report TN 182, NACA 1924
[11] Pistolesi E. Il Problema dell'ala in Vicinanza del Suolo. L'Aerotecnica 1933, Vol. 13(4)
[12] Pistolesi E. Ground effect-theory and practice. NACA TM 828, 1937
[13] Frediani A., Cipolla V., Abu Salem K., Binante V., Scardaoni Picchi M., Conceptual design of PrandtlPlane civil transport aircraft, 2019. Conceptual design of PrandtlPlane civil transport aircraft. Proceedings of the Institution of Mechanical Engineers, Part G: Journal of Aerospace Engineering.
[14] Cipolla, V., A. Frediani, K. Abu Salem, M. Picchi Scardaoni, A. Nuti, V. Binante. 2018. Conceptual design of a box wing aircraft for the air transport of the future. AIAA Aviation Forum.
[15] K. Abu Salem, V. Binante, V. Cipolla, M. Maganzi, PARSIFAL Project: a breakthrough innovation in air transport, Aerotecnica MIssili&Spazio, 2018
[16] K. Abu Salem, V. Cipolla, M. Carini, M. Méheut, S. Kanellopoulos, V. Binante, M. Maganzi, Aerodynamic design and preliminary optimization of a commercial PrandtlPlane aircraft, 8th EUCASS conference, 2019
[17] Requirements for the adoption of the PrandtlPlane as a mean of transport. Deliverable 2.1, PARSIFAL Project, 2018, www.parsifalproject.eu
[18] CeRAS - Central Reference Aircraft System. www.ceras.ilr.rwthaachen.de/trac/wiki/CeRAS/AircraftDesigns/CSR01
[19] Torenbeek E., Synthesis of subsonic airplane design. ISBN 978-90-247-2724-7; 1982. Springer.
[20] Bianchi M., Analysis of take-off performance of a Prandtlplane 300 seat civil transport aircraft. University of Pisa, 2018
[21] Airbus, A.G. Getting to grips with aircraft performance. Cust. Serv. Blagnac 2002